Journal of Medicinal Chemistry

Article

pubs.acs.org/jmc

Structural Analysis of Bengamide Derivatives as Inhibitors of Methionine Aminopeptidases

Wei Xu, Jing-Ping Lu, and Qi-Zhuang Ye*

Department of Biochemistry and Molecular Biology, Indiana University School of Medicine, Indianapolis, Indiana 46202, United States

ABSTRACT: Natural-product-derived bengamides possess potent antiproliferative activity and target human methionine aminopeptidases (MetAPs) for their cellular effects. Several derivatives were designed, synthesized, and evaluated as MetAP inhibitors. Here, we present four new X-ray structures of human MetAP1 in complex with the inhibitors. Together with the previous structures of bengamide derivatives with human MetAP2 and tubercular *Mt*MetAP1c, analysis of the interactions of these inhibitors at the active site provides structural basis for further modification of these bengamide inhibitors for improved potency and selectivity as anticancer and antibacterial therapeutics.

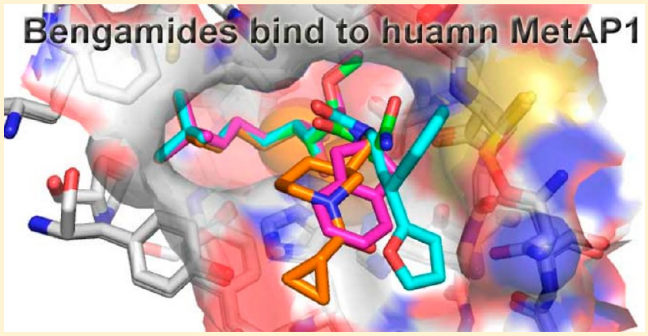

INTRODUCTION

Bengamides are natural products that were isolated from marine sponge.[1] Bengamides A and B (**1** and **2** in Figure 1) showed antiproliferative activity with nanomolar potency against cancer cell lines,[2,3] and bengamides arrest mammalian cells at the G1 and G2/M phases of the cell cycle.[2,4] The cellular targets of bengamides were identified as two human methionine aminopeptidases (*Hs*MetAP1 and *Hs*MetAP2) by a proteomic approach.[5] Bengamides inhibit the two human MetAP isozymes with similar potencies.[5]

MetAP is ubiquitous and carries out N-terminal methionine excision from a majority of newly synthesized proteins.[6] The importance of this cotranslational modification is underscored by the observed lethality when the single MetAP gene is deleted in bacteria, such as *Escherichia coli*[7] and *Salmonella typhimurium*.[8] Therefore, MetAP is a potential target for developing novel antibacterial drugs.[9] Eukaryotic cells usually have two MetAPs, type 1 and type 2. Deletion of either of the two MetAP genes in *Saccharomyces cerevisiae* rendered a slow growth phenotype, and lethality was observed when both genes were deleted.[10] Mammalian MetAP1 and MetAP2 play important roles in cell proliferation and angiogenesis,[11,12] and by use of a conditional MetAP2 knockout mouse, the gene disruption resulted in an embryonic gastrulation defect and endothelial cell growth arrest.[13] Fumagillin is another natural product that inhibits angiogenesis and suppresses tumor growth,[14] and it targets MetAP2 enzyme specifically.[11,15] Clinical trials have been carried out for anticancer therapy, using the synthetic bengamide derivative LAF389 (**3**)[16] and a fumagillin derivative.[17,18]

The unique bound conformation of bengamides at the MetAP active site was first revealed by the X-ray structure of the human enzyme *Hs*MetAP2 in complex with a bengamide derivative LAF153 (**4**) (PDB code 1QZY, Figure 2A).[5] In the dimetalated structure, the triol moiety of **4** coordinates with the two Co(II) ions to form two octahedral geometries, which is reminiscent of the binding of a bestatin-derived transition state inhibitor.[19] The spatial arrangement of three hydroxyl groups may uniquely satisfy the coordination requirement and possibly confer the high affinity. The *tert*-butylalkene substituent occupies the site often seen for the terminal methionine in a peptide substrate, and on the other side of the triol moiety, a caprolactam ring beyond the amide bond interacts with residues toward the opening of the active site pocket. This unique binding mode of bengamides has guided our design and synthesis of several bengamide derivatives (**5**−**9**), and some of them displayed potent inhibition of the *Mycobacterium tuberculosis* MetAPs (*Mt*MetAP1a and *Mt*MetAP1c) and modest antitubercular activity.[20]

Human *Hs*MetAP1 regulates cell cycle and is a promising target for the discovery and development of new anticancer agents.[12] However, although bengamides inhibit *Hs*MetAP1 potently,[5] there is currently no structural information for binding of bengamides. In fact, there are only seven X-ray structures of *Hs*MetAP1 found in the PDB databank and only four structures with a ligand bound at the active site.[12,21,22] Here, we report four new X-ray structures of *Hs*MetAP1 in complex with four different bengamide derivatives (**5**, **7**−**9**), and the binding mode of bengamides in these structures is significantly different from those in the previous *Hs*MetAP1 structures. Recently, we reported five X-ray structures of the tubercular *Mt*MetAP1c in complex with the bengamides **5**−**8** (PDB codes 3PKA, 3PKB, 3PKC, 3PKD, 3PKE).[20,23] Together, the structural information of bengamides at the active site of different MetAP enzymes provides guidance for using bengamides as a template for designing potent and selective MetAP inhibitors for antibacterial and anticancer therapeutics.

Received: June 20, 2012
Published: August 22, 2012

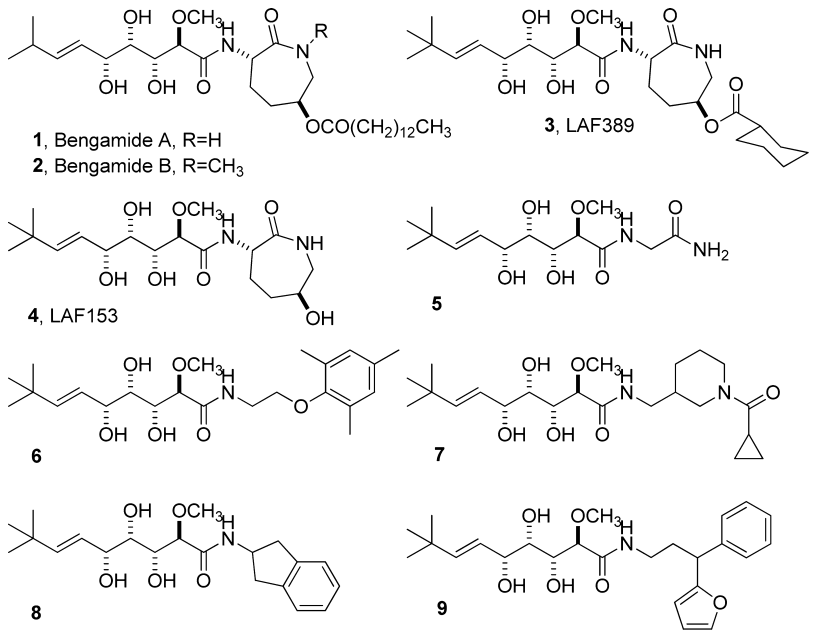

Figure 1. Chemical structures of natural bengamides (**1** and **2**) and their synthetic derivatives reported in the literature (**3** and **4**) and designed and synthesized in this laboratory (**5**–**9**).

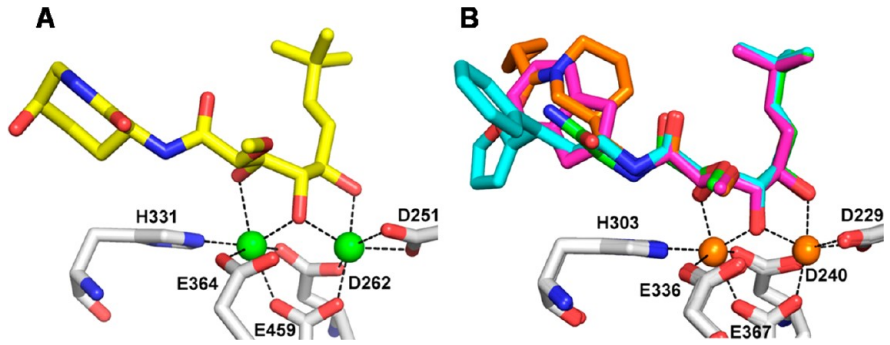

Figure 2. Coordination of bengamide derivatives with the metal ions at the dinuclear catalytic site: (A) inhibitor **4** with two Co(II) ions in *Hs*MetAP2; (B) inhibitors **5** and **7**–**9** with two Mn(II) ions in *Hs*MetAP1. Inhibitors and protein residues are shown as sticks, and metal ions are shown as spheres. Coordination between the metal ions and the heteroatoms of the inhibitors or protein residues is shown as dashed lines. Only metal coordinating protein residues are shown. For coloring of carbon atoms, **4** is yellow, **5** is green, **7** is orange, **8** is magenta, **9** is cyan, and protein residues are gray. For coloring of non-carbon atoms, oxygen is red and nitrogen is blue. For coloring of the metal ions, Co(II) is green and Mn(II) is orange.

RESULTS AND DISCUSSION

X-ray Structures of HsMetAP1 in Complex with 5, 7, 8, or 9. Four X-ray structures of *Hs*MetAP1 in complex with four different bengamide derivatives **5**, **7**, **8**, and **9** in the Mn(II) form were solved at high resolution (1.47–1.75 Å) (Table 1, Figure 2B and Figure 3) from crystals obtained individually by cocrystallization. As seen before on *Mt*MetAP1c[20,23] and on *Hs*MetAP2,[5] these bengamides bound to *Hs*MetAP1 similarly for part of the molecules including the triol moiety and the *tert*-butylalkene chain. The triol moiety coordinated with the two active site metal ions, and the *tert*-butylalkene chain occupied the S1 site. However, each of the bengamide derivatives bound significantly differently from **4** at the amide moiety, exploring different interactions at the opening of the active site pocket due to different amide structures.

Clear electron density was seen surrounding the whole molecule of inhibitor **5** (Figure 3A). However, for inhibitors **7**, **8**, and **9**, although the density is clear on the *tert*-butylalkene moiety and the triol moiety, the density is not as clear on the amide moiety at this contour level (Figure 3B–D). This is consistent with the smaller average *B*-factor (17.5) for inhibitor **5** in comparison with those for **7**, **8**, and **9** (30.6, 22.7, and 27.6, respectively). However, this observation of lack of electron density to cover the part of amide moieties is unique to *Hs*MetAP1 because in the recently solved structures of *Mt*MetAP1c in complex with **7** or **8**, the density was clear all over the inhibitor molecules.[23] Therefore, this lack of density indicates mobility and poor binding of the amide moiety at the opening of the pocket. Indeed, all of these bengamide derivatives have similar potencies in inhibiting the Mn(II) form of *Hs*MetAP1 (IC_{50}: **5**, 3.59 μM; **7**, 7.45 μM; **8**, 5.58 μM; **9**, 5.14 μM), suggesting that the major contributors of the bengamide binding to *Hs*MetAP1 are from the *tert*-butylalkene moiety and the triol moiety. It is interesting to note that in the structure of *Hs*MetAP2 (PDB code 1QZY), the average *B*-factor (23.4 ± 1.7) for non-hydrogen atoms in the amide moiety of the inhibitor molecule **4** is clearly larger than that (19.8 ± 1.4) for atoms in other parts. Compound **4** is the one used in structural determination, and compared with the clinically

dx.doi.org/10.1021/jm3008695 | J. Med. Chem. 2012, 55, 8021–8027

Table 1. X-ray Data Collection and Refinement Statistics

	inhibitor			
	5	**7**	**8**	**9**
inhibitor code	Y16	Y08	Y10	YZ6
PDB code	4FLI	4FLJ	4FLK	4FLL
		Cell Parameters		
space group	$P2_1$	$P2_1$	$P2_1$	$P2_1$
a (Å)	47.8	48.0	47.8	47.8
b (Å)	77.6	77.4	77.5	77.1
c (Å)	48.8	48.5	48.6	48.6
α (deg)	90	90	90	90
β (deg)	90.2	90.0	90.4	90.2
γ (deg)	90	90	90	90
		X-ray Data Collection		
resolution range (Å)[a]	50−1.56 (1.59−1.56)	50−1.75 (1.78−1.75)	50−1.47 (1.50−1.47)	50−1.50 (1.53−1.50)
collected reflections	185 568	130 604	215 352	209 851
unique reflections	50 632	35 919	60 021	55 956
completeness (%)[a]	99.8 (99.3)	99.9 (99.5)	99.5 (96.1)	99.9 (100)
$I/\sigma(I)$ [a]	36.1 (2.5)	30.1 (2.2)	41.9 (4.0)	34.2 (3.0)
R_{merge} (%)[a]	9.6 (53.4)	8.9 (56.2)	9.5 (38.5)	9.5 (53.9)
		Refinement Statistics		
R (%)	18.3	19.8	19.9	18.0
R_{free} (%)	21.1	23.2	22.1	21.3
rmsd bonds (Å)	0.030	0.025	0.031	0.030
rmsd angles (deg)	2.38	2.02	2.43	2.50
no. of solvent molecules	184	137	154	213
$\langle B \rangle$ protein (Å^2)	22.4	27.9	22.3	21.1
$\langle B \rangle$ inhibitor (Å^2)	17.5	30.6	22.7	27.6
$\langle B \rangle$ water (Å^2)	28.6	30.8	27.3	29.3

[a]Values given in parentheses correspond to the outer shell of data.

tested **3**, it lacks the cyclohexanecarboxyl group, which may be needed for enhanced binding and activity. Clearly, the substitution on the seven-membered caprolactam ring had significant influence on in vitro and in vivo activities of these bengamide derivatives.[2] Similarly for our bengamide derivatives **5**−**9**, the X-ray structures revealed their binding modes on MetAPs and provided the directions for further modifications. Substitutions to extend the amide moiety will likely allow exploration of additional interactions and enhancement of their binding to their targeting MetAPs.

Structurally Mobile Loop in HsMetAP1 at the Vicinity of the Binding Pocket. When we built the structures, it was difficult to model the loop of K132, G133, and T134 in all of these *Hs*MetAP1 structures. Considering the closeness of this loop to the active site, it is questionable whether this difficulty is related to the lack of density around the amide moiety of inhibitors mentioned above. The final structures have much larger *B*-factors for these three residues (Figure 4A and Figure 4C, indicated by an arrow). This led us to reexamine the seven previously obtained *Hs*MetAP1 structures (2B3H, 2B3K, 2B3L, 2G6P, 2GZ5, 2NQ6, and 2NQ7). Indeed, in all *Hs*MetAP1 structures, with or without a ligand, these residues have larger *B*-factors, indicating that their mobility is a common feature in *Hs*MetAP1 structures.

All MetAPs are homologous in sequence in the catalytic domain, and *E. coli* MetAP1 (*Ec*MetAP1) is a typical bacterial MetAP and the smallest with only the catalytic domain (Figure 4B). On the other hand, mammalian MetAPs, including *Hs*MetAP1 and *Hs*MetAP2, have an extension at the N-terminus.[10,24] *S. cerevisiae* MetAP1 has two zinc fingers in the extension, and the zinc fingers are essential for normal MAP function in vivo, even though the in vitro enzyme assays indicate that they are not involved in catalysis.[25] It is interesting to note that when bacterial MetAPs and mammalian MetAPs are aligned by sequence, this mobile loop is located right at the junction of the catalytic domain and the N-terminal extension. When *Hs*MetAP1 was expressed in *E. coli*, the full length enzyme was obtained but not stable during purification and storage, and N-terminal truncations were observed.[26] All *Hs*MetAP1 structures so far, including ours, start at the N-terminus around Y90, and the structure of a full length *Hs*MetAP1 remains elusive. The mobility of the K132−G133−T134 loop may partially contribute to the instability of protein. Similarly, in all *Hs*MetAP2 structures, the N-terminus is missing before K110, and the junction (around T151) of the N-terminal extension and the catalytic domain was either invisible (Figure 4E, indicated by a dotted line) or showed much larger *B*-factors.

The function of the N-terminal extension in MetAP1 and MetAP2 is not clear, and it is not clear whether the truncated forms exist in vivo. Previously, we prepared and characterized truncated *Hs*MetAP1(Δ1−66) and *Hs*MetAP1(Δ1−135) in *E. coli*.[26] Although the N-terminal extension in *Hs*MetAP1 is not required for enzyme activity, it has a significant impact on interaction of the enzyme with its substrates and inhibitors.[26] *Mycobacterium tuberculosis* is a mycobacterium, and *Mt*MetAP1c has a shorter N-terminal extension. Compared with *Hs*MetAP1, similarly located residues in *Mt*MetAP1c showed no such mobility as indicated by much tighter *B*-factors in the region (Figure 4D). Addlagatta et al. noticed that despite the structural and sequence changes in this extension, there are two spatially conserved residues (Y117 and E128 in *Hs*MetAP1, and Y27 and E35 in *Mt*MetAP1c) that form hydrogen bonds and

dx.doi.org/10.1021/jm3008695 | J. Med. Chem. 2012, 55, 8021−8027

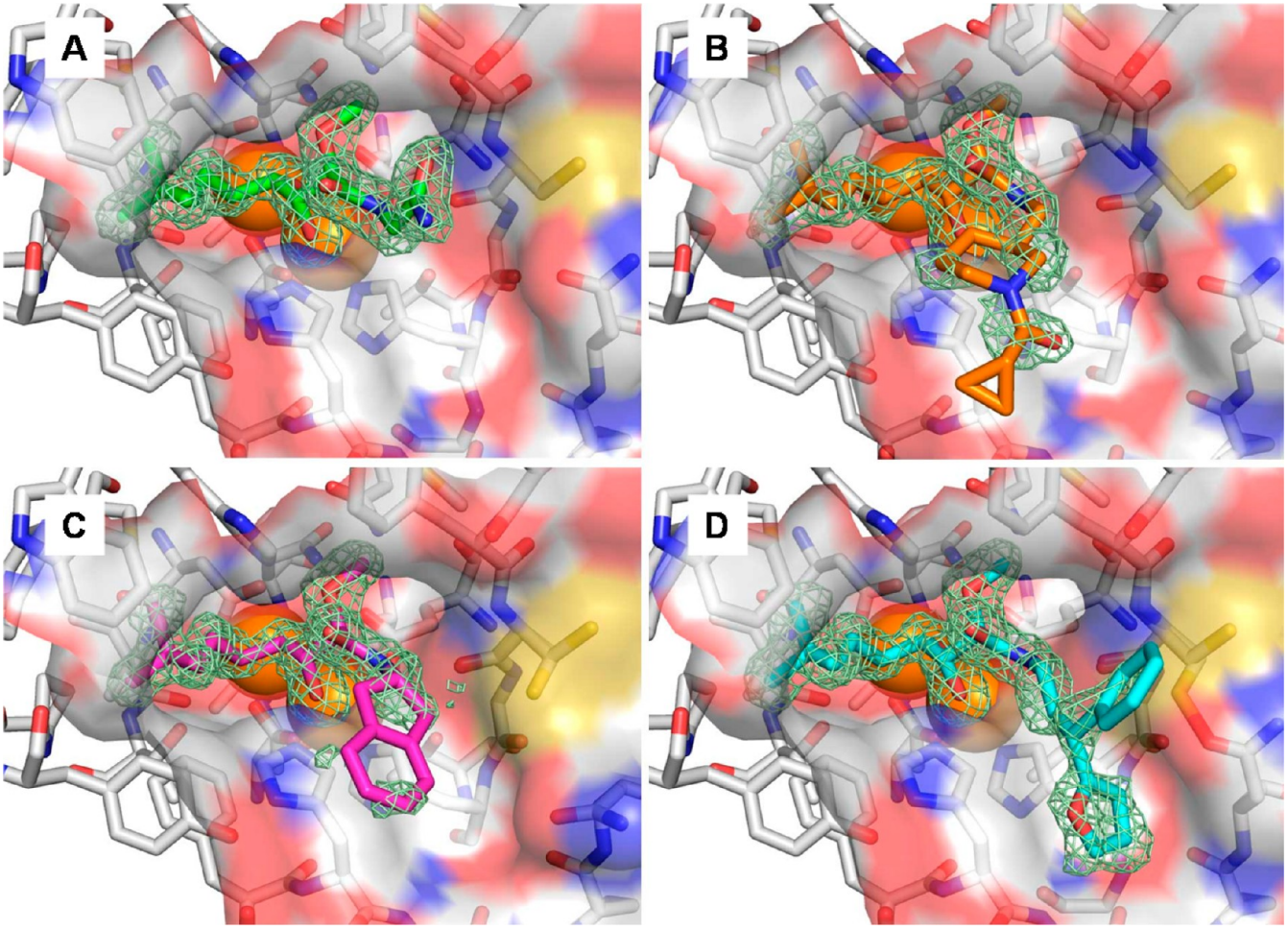

Figure 3. Binding of the bengamide derivatives **5** (A), **7** (B), **8** (C), and **9** (D) at the active site pocket of *Hs*MetAP1. The inhibitors and protein residues (sticks) and the Mn ions (spheres) are colored in the same scheme as in Figure 2. The semitransparent surface formed by protein residues is colored gray for carbon, red for oxygen, and blue for nitrogen. $F_{obs} - F_{calc}$ omit maps (inhibitors were omitted in the models) are shown superimposed on the refined structures as light green meshes contoured at 3σ.

hydrophobic interactions with residues that help form the substrate-binding pocket (S191, Y195, F309, and H310 in *Hs*MetAP1, and S93, Y97, and F211 in *Mt*MetAP1c).[27] The mobility of the K132−G133−T134 loop extends at least to E128, and their mobility may affect the binding of substrates and inhibitors directly or indirectly. We observed significant differences in catalysis and inhibition between full-length and truncated *Hs*MetAP1s.[26]

Similarities and Differences in Binding of Bengamide Derivatives on HsMetAP1, HsMetAP2, and MtMetAP1c. Five residues that coordinate to the two metal ions at the active site (D97, D108, H171, E204, and E235 in *Ec*MetAP1, Table 2) and two catalytically involved histidine residues are conserved in all MetAPs. When the structures of *Hs*MetAP1, *Hs*MetAP2, and *Mt*MetAP1c are superimposed, the bengamides **4** and **5** showed the same binding mode on the three different MetAP enzymes (Figure 5). Apparently, the two metal ions dictate the conformation of the metal coordinating residues and the triol moiety of the bengamide inhibitors. With the triol moiety in the middle of the linear inhibitors fixed at the metal site, other parts of the inhibitors had little variation in the bound conformation.

Type 1 MetAPs are more homologous in the active site pocket, and most residues that form the pocket are either identical or conserved (Table 2). This presents a challenge in developing selective inhibitors for antibacterial purposes that can differentiate bacterial MetAPs and *Hs*MetAP1 because they all belong to type 1 MetAP. However, at the opening and outside of the pocket, more structural variations exist for type 1 MetAPs (Figure 6), and extending the bengamide derivatives to explore additional interactions will potentially increase not only potency on bacterial MetAPs but also selectivity. The carbonyl group used to form the amide moiety in bengamides is properly located and provides a chemical handle for chemical modifications by attaching different amino-containing substitutions.

Both *Hs*MetAP1 and *Hs*MetAP2 are potential targets for developing anticancer drugs. However, because of the important function played by MetAP in normal cells, it is possible but unknown whether selective inhibition of one of the two human MetAP enzymes will provide any therapeutic or toxicological benefits. Besides the two well-studied human MetAPs, there is another less-known human MetAP named MetAP1D, which is of mitochondrial origin.[28] It was only biochemically characterized,[29] and its structural information is not available. Therefore, selective inhibitors of human MetAPs are desired to provide the research tools to elucidate the mechanism of individual human MetAP in cancer pathogenesis and to generate novel leads as anticancer agents. Because of the insertion in the catalytic domain in

dx.doi.org/10.1021/jm3008695 | *J. Med. Chem.* 2012, 55, 8021−8027

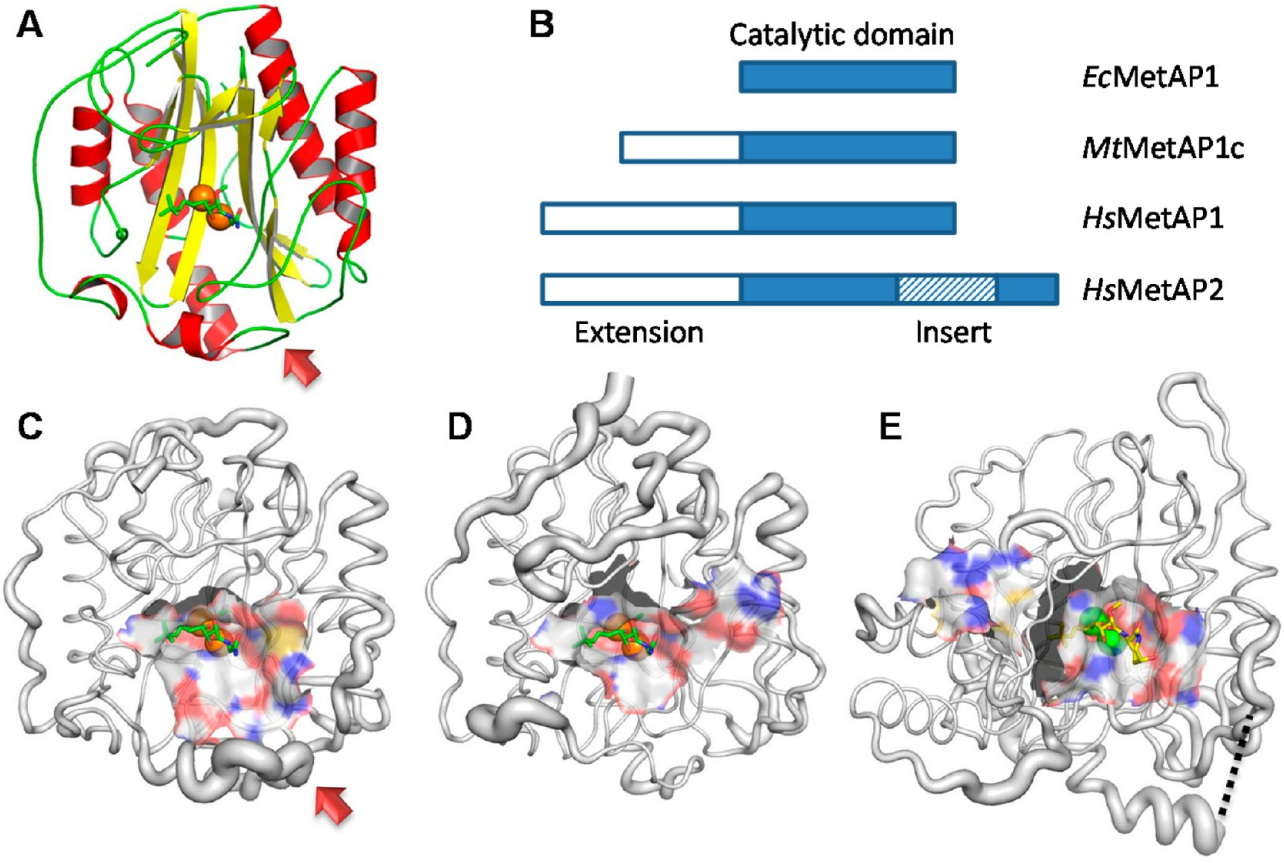

Figure 4. Flexible K132−G133−T134 loop in *Hs*MetAP1 at the junction of the catalytic domain and the N-terminal extension. The structure of *Hs*MetAP1 with **5** is shown as ribbon drawing (A) and as putty drawing (C) with the tube diameters proportional to *B*-factors. For comparison, the structures of *Mt*MetAP1c with **5** (D) and *Hs*MetAP2 with **4** (E) are also shown as putty drawings. The active site is shown as semitransparent surfaces with the inhibitor and metal ions. The flexible loop in human MetAP1 is indicated by an arrow in parts Aand C. The junction residues in *Hs*MetAP2 are invisible in 1QZY and indicated by a dotted line in part E. All of the structures were adjusted to similar orientations with the same color scheme as in Figure 2. *Hs*MetAP1 belongs to type 1 MetAP, as *Ec*MetAP1 and *Mt*MetAP1c, while *Hs*MetAP2 belongs to type 2 MetAP with a typical insert for MetAP2, and their domain structures are shown in part B.

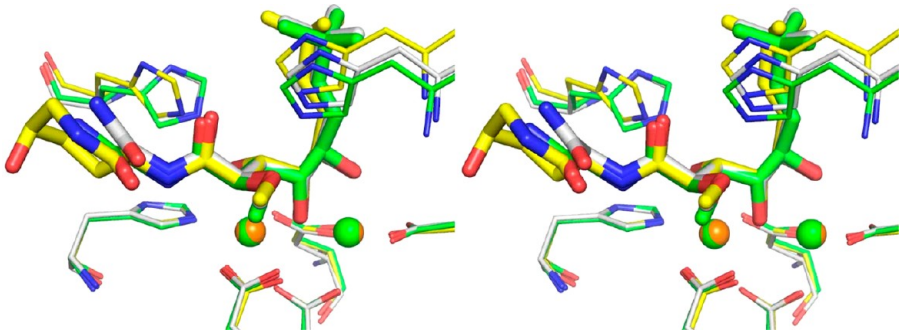

Figure 5. Stereoview of the superimposed bengamide derivatives **5** (with *Hs*MetAP1, carbon green; with *Mt*MetAP1c, carbon gray) and **4** (with *Hs*MetAP2, carbon yellow) at the active site with coordination to catalytic metal ions (shown as green or orange spheres). The left panel and the right panel are a stereopair, and one was rotated 6° to the other along *z* axis for viewing in stereo. The inhibitors are thicker sticks, and the protein residues are thinner sticks. Only five metal-coordinating residues and two catalytically important histidine residues (see Table 2) are shown.

*Hs*MetAP2 (Figure 4B), the residues forming the active site pocket are not paired well between *Hs*MetAP1 and *Hs*MetAP2 (Table 2) except the metal coordinating residues and two conserved histidine residues. This variation in the active site pocket provides opportunities to explore the differences for selectivity. In addition, significant differences exist outside the pocket (Figure 6B and Figure 6C) for exploration for increased potency and selectivity.

In conclusion, natural bengamides and synthetic bengamide derivatives are inhibitors of MetAPs, and their unique binding modes make them an ideal template for developing potent and selective MetAP inhibitors as therapeutics. The X-ray structures of MetAP enzymes in complex with different bengamide derivatives provide the valuable structural information for such inhibitor development.

■ EXPERIMENTAL SECTION

Compounds used in the experiments were synthesized in this laboratory and were at least 95% pure on the basis of HPLC−MS.[20] Proteins

dx.doi.org/10.1021/jm3008695 | *J. Med. Chem.* 2012, 55, 8021−8027

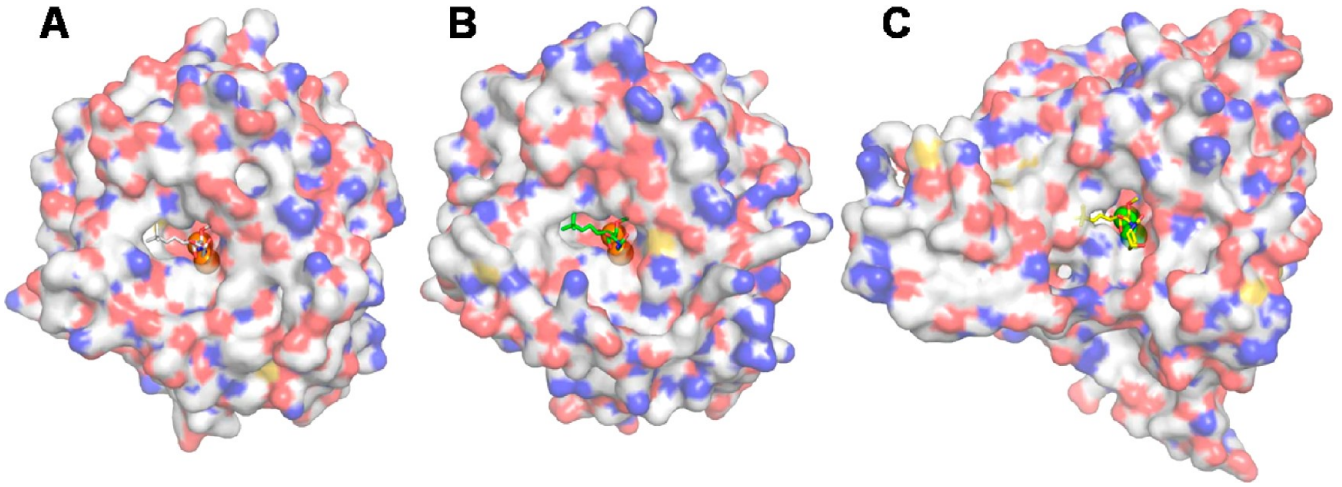

Figure 6. Overall structures of *Mt*MetAP1c with **5** bound (A), *Hs*MetAP1 with **5** bound (B), and *Hs*MetAP2 with **4** bound (**C**), shown as surface drawing (carbon, gray; nitrogen, blue; and oxygen, red). Inhibitors are colored the same as in Figure 5.

Table 2. Residues within 4 Å of the Bengamide Inhibitors in the Active Site Pocket

type 1			
*Hs*MetAP1	*Mt*MetAP1c	*Ec*MetAP1[a]	type 2 *Hs*MetAP2[b]
Residues of Metal Ligation			
H303	H205	H171	H331
D240	D142	D108	D262
E367	E269	E235	E459
E336	E238	E204	E364
D229	D131	D97	D251
Two Conserved Histidines			
H310	H212	H178	H339
H212	H114	H79	H231
Other Active Site Residues			
W353	W255	W221	
Y195	Y97	Y62	
F309	F211	F177	
T231	T133	T99	
C203	C105	C70	
C211	C113	C78	A230
C301	T203	C169	N329
Y300	F202	Y168	L328
P192	T94	C59	
N314	V216	Q182	T343

[a]Because no structure of *Ec*MetAP1 with a bengamide has been obtained, listed are the similarly located residues. [b]For *Hs*MetAP2, only residues that occur at corresponding positions in space in *Hs*MetAP1 are listed in the same horizontal line.

were expressed in *E. coli* and purified to homogeneity as previously described with minor modifications.[26] Crystals of the enzyme–inhibitor complexes were obtained independently by microbath method under paraffin oil at room temperature. Each of the inhibitors (**5**, **7**, **8**, and **9**; 100 mM in DMSO) was added to concentrated metalated enzyme (10 mg/mL, 0.27 mM protein; 0.675 mM metal) in 20 mM Tris, pH 8.0, and 100 mM NaCl, 2 mM DTT, and the molar ratio of inhibitor to *Hs*MetAP1 was 5:1. The enzyme/inhibitor mixture was mixed with a reservoir buffer in a 1:1 ratio. The reservoir buffer was 200 mM sodium acetate, pH 8.0, and 20% PEG 3350 for **5**, **7**, and **9** and 200 mM sodium formate, pH 7.2, and 20% PEG 3350 for **8**. Diffraction data were collected at the Advanced Photon Source, Argonne National Laboratory (beamlines 19BM and 19ID) and processed with HKL3000.[30] The crystals belong to space group $P2_1$. In each case, one molecule is in the asymmetric unit. The structures were solved by molecular replacement with MolRep[31] in CCP4[32] with CCP4i interface,[33] using the previously published *Hs*MetAP1 structure (PDB code 2NQ6)[34] as the search model. The structure was refined with REFMAC5[35] with iterative model building using WinCoot.[36] The refinement was monitored with 5% of the reflections set aside for R_{free} factor analysis throughout the whole refinement process. Electron density was clear for all residues except a few residues at the N-terminus, and residues from Y90 in the native protein to the S393, third residue from the C-terminus, were modeled. Comparison of structures and generation of structural drawings were carried out by using PyMOL.[37] Statistic parameters in data collection and structural refinement are shown in Table 1. Atomic coordinates and structure factors for the four structures were deposited in the Protein Data Bank.

■ ASSOCIATED CONTENT

Accession Codes

PDB codes for compounds **5**, **7**, **8**, and **9** are 4FLI, 4FLJ, 4FLK, and 4FLL, respectively.

■ AUTHOR INFORMATION

Corresponding Author

*Telephone: 317-278-0304. E-mail: yeq@iupui.edu.

Notes

The authors declare no competing financial interest.

■ ACKNOWLEDGMENTS

This work was supported by National Institutes of Health Grants R01 AI065898 and R56 AI065898 and by Indiana University School of Medicine (BRG), Indiana University and Purdue University at Indianapolis (RSFG), and the Experimental and Developmental Therapeutics Program at the IU Simon Cancer Center (ITRAC) (to Q.-Z.Y.). We thank the staff at Structural Biology Center of the Advanced Photon Source, Argonne National Laboratory (beamlines 19BM and 19ID), for assistance with data collection.

■ ABBREVIATIONS USED

MetAP, methionine aminopeptidase; *Hs*MetAP1, human MetAP type 1; *Hs*MetAP2, human MetAP type 2; *Mt*MetAP1a, *M. tuberculosis* MetAP type 1a; *Mt*MetAP1c, *M. tuberculosis* MetAP type 1c; *Ec*MetAP1, *E. coli* MetAP type 1; IC_{50}, concentration of 50% inhibition

REFERENCES

(1) Quinoa, E.; Adamczeski, M.; Crews, P.; Bakus, G. J. Bengamides, heterocyclic anthelmintics from a Jaspidae marine sponge. *J. Org. Chem.* **1986**, *51*, 4494−4497.

(2) Kinder, F. R., Jr.; Versace, R. W.; Bair, K. W.; Bontempo, J. M.; Cesarz, D.; Chen, S.; Crews, P.; Czuchta, A. M.; Jagoe, C. T.; Mou, Y.; Nemzek, R.; Phillips, P. E.; Tran, L. D.; Wang, R. M.; Weltchek, S.; Zabludoff, S. Synthesis and antitumor activity of ester-modified analogues of bengamide B. *J. Med. Chem.* **2001**, *44*, 3692−3699.

(3) Thale, Z.; Kinder, F. R.; Bair, K. W.; Bontempo, J.; Czuchta, A. M.; Versace, R. W.; Phillips, P. E.; Sanders, M. L.; Wattanasin, S.; Crews, P. Bengamides revisited: new structures and antitumor studies. *J. Org. Chem.* **2001**, *66*, 1733−1741.

(4) Phillips, P. E.; Bair, K. W.; Bontempo, J.; Crews, P.; Czuchta, M., A.; Kinder, F. R.; Vattay, A.; Versace, R. W.; Wang, B.; Wang, J.; Wood, A.; Zabludoff, S. Bengamide E arrests cells at the G1/S restriction point and within the G2/M phase of the cell cycle. *Proc. Am. Assoc. Cancer Res.* **2000**, *41*, 59.

(5) Towbin, H.; Bair, K. W.; DeCaprio, J. A.; Eck, M. J.; Kim, S.; Kinder, F. R.; Morollo, A.; Mueller, D. R.; Schindler, P.; Song, H. K.; van Oostrum, J.; Versace, R. W.; Voshol, H.; Wood, J.; Zabludoff, S.; Phillips, P. E. Proteomics-based target identification: bengamides as a new class of methionine aminopeptidase inhibitors. *J. Biol. Chem.* **2003**, *278*, 52964−52971.

(6) Giglione, C.; Boularot, A.; Meinnel, T. Protein N-terminal methionine excision. *Cell. Mol. Life Sci.* **2004**, *61*, 1455−1474.

(7) Chang, S. Y.; McGary, E. C.; Chang, S. Methionine aminopeptidase gene of *Escherichia coli* is essential for cell growth. *J. Bacteriol.* **1989**, *171*, 4071−4072.

(8) Miller, C. G.; Kukral, A. M.; Miller, J. L.; Movva, N. R. pepM is an essential gene in *Salmonella typhimurium*. *J. Bacteriol.* **1989**, *171*, 5215−5217.

(9) Vaughan, M. D.; Sampson, P. B.; Honek, J. F. Methionine in and out of proteins: targets for drug design. *Curr. Med. Chem.* **2002**, *9*, 385−409.

(10) Li, X.; Chang, Y. H. Amino-terminal protein processing in *Saccharomyces cerevisiae* is an essential function that requires two distinct methionine aminopeptidases. *Proc. Natl. Acad. Sci. U.S.A.* **1995**, *92*, 12357−12361.

(11) Griffith, E. C.; Su, Z.; Turk, B. E.; Chen, S.; Chang, Y. H.; Wu, Z.; Biemann, K.; Liu, J. O. Methionine aminopeptidase (type 2) is the common target for angiogenesis inhibitors AGM-1470 and ovalicin. *Chem. Biol.* **1997**, *4*, 461−471.

(12) Hu, X.; Addlagatta, A.; Lu, J.; Matthews, B. W.; Liu, J. O. Elucidation of the function of type 1 human methionine aminopeptidase during cell cycle progression. *Proc. Natl. Acad. Sci. U.S.A.* **2006**, *103*, 18148−18153.

(13) Yeh, J. R.; Ju, R.; Brdlik, C. M.; Zhang, W.; Zhang, Y.; Matyskiela, M. E.; Shotwell, J. D.; Crews, C. M. Targeted gene disruption of methionine aminopeptidase 2 results in an embryonic gastrulation defect and endothelial cell growth arrest. *Proc. Natl. Acad. Sci. U.S.A.* **2006**, *103*, 10379−10384.

(14) Ingber, D.; Fujita, T.; Kishimoto, S.; Sudo, K.; Kanamaru, T.; Brem, H.; Folkman, J. Synthetic analogues of fumagillin that inhibit angiogenesis and suppress tumour growth. *Nature* **1990**, *348*, 555−557.

(15) Sin, N.; Meng, L.; Wang, M. Q.; Wen, J. J.; Bornmann, W. G.; Crews, C. M. The anti-angiogenic agent fumagillin covalently binds and inhibits the methionine aminopeptidase, MetAP-2. *Proc. Natl. Acad. Sci. U.S.A.* **1997**, *94*, 6099−6103.

(16) Dumez, H.; Gall, H.; Capdeville, R.; Dutreix, C.; van Oosterom, A. T.; Giaccone, G. A phase I and pharmacokinetic study of LAF389 administered to patients with advanced cancer. *Anti-Cancer Drugs* **2007**, *18*, 219−225.

(17) Bhargava, P.; Marshall, J. L.; Rizvi, N.; Dahut, W.; Yoe, J.; Figuera, M.; Phipps, K.; Ong, V. S.; Kato, A.; Hawkins, M. J. A phase I and pharmacokinetic study of TNP-470 administered weekly to patients with advanced cancer. *Clin. Cancer Res.* **1999**, *5*, 1989−1995.

(18) Logothetis, C. J.; Wu, K. K.; Finn, L. D.; Daliani, D.; Figg, W.; Ghaddar, H.; Gutterman, J. U. Phase I trial of the angiogenesis inhibitor TNP-470 for progressive androgen-independent prostate cancer. *Clin. Cancer Res.* **2001**, *7*, 1198−1203.

(19) Lowther, W. T.; Orville, A. M.; Madden, D. T.; Lim, S.; Rich, D. H.; Matthews, B. W. *Escherichia coli* methionine aminopeptidase: implications of crystallographic analyses of the native, mutant, and inhibited enzymes for the mechanism of catalysis. *Biochemistry* **1999**, *38*, 7678−7688.

(20) Lu, J. P.; Yuan, X. H.; Yuan, H.; Wang, W. L.; Wan, B.; Franzblau, S. G.; Ye, Q. Z. Inhibition of *Mycobacterium tuberculosis* methionine aminopeptidases by bengamide derivatives. *ChemMedChem* **2011**, *6*, 1041−1048.

(21) Hu, X.; Addlagatta, A.; Matthews, B. W.; Liu, J. O. Identification of pyridinylpyrimidines as inhibitors of human methionine aminopeptidases. *Angew. Chem., Int. Ed.* **2006**, *45*, 3772−3775.

(22) Addlagatta, A.; Matthews, B. W. Structure of the angiogenesis inhibitor ovalicin bound to its noncognate target, human type 1 methionine aminopeptidase. *Protein Sci.* **2006**, *15*, 1842−1848.

(23) Lu, J. P.; Yuan, X. H.; Ye, Q. Z. Structural analysis of inhibition of *Mycobacterium tuberculosis* methionine aminopeptidase by bengamide derivatives. *Eur. J. Med. Chem.* **2012**, *47*, 479−484.

(24) Arfin, S. M.; Kendall, R. L.; Hall, L.; Weaver, L. H.; Stewart, A. E.; Matthews, B. W.; Bradshaw, R. A. Eukaryotic methionyl aminopeptidases: two classes of cobalt-dependent enzymes. *Proc. Natl. Acad. Sci. U.S.A.* **1995**, *92*, 7714−7718.

(25) Zuo, S.; Guo, Q.; Ling, C.; Chang, Y. H. Evidence that two zinc fingers in the methionine aminopeptidase from *Saccharomyces cerevisiae* are important for normal growth. *Mol. Gen. Genet.* **1995**, *246*, 247−253.

(26) Li, J. Y.; Chen, L. L.; Cui, Y. M.; Luo, Q. L.; Gu, M.; Nan, F. J.; Ye, Q. Z. Characterization of full length and truncated type I human methionine aminopeptidases expressed from *Escherichia coli*. *Biochemistry* **2004**, *43*, 7892−7898.

(27) Addlagatta, A.; Hu, X.; Liu, J. O.; Matthews, B. W. Structural basis for the functional differences between type I and type II human methionine aminopeptidases. *Biochemistry* **2005**, *44*, 14741−14749.

(28) Leszczyniecka, M.; Bhatia, U.; Cueto, M.; Nirmala, N. R.; Towbin, H.; Vattay, A.; Wang, B.; Zabludoff, S.; Phillips, P. E. MAP1D, a novel methionine aminopeptidase family member is overexpressed in colon cancer. *Oncogene* **2006**, *25*, 3471−3478.

(29) Hu, X. V.; Chen, X.; Han, K. C.; Mildvan, A. S.; Liu, J. O. Kinetic and mutational studies of the number of interacting divalent cations required by bacterial and human methionine aminopeptidases. *Biochemistry* **2007**, *46*, 12833−12843.

(30) Minor, W.; Cymborowski, M.; Otwinowski, Z.; Chruszcz, M. HKL-3000: the integration of data reduction and structure solution—from diffraction images to an initial model in minutes. *Acta Crystallogr., Sect. D: Biol. Crystallogr.* **2006**, *62*, 859−866.

(31) Vagin, A.; Teplyakov, A. MOLREP: an automated program for molecular replacement. *J. Appl. Crystallogr.* **1997**, *30*, 1022−1025.

(32) Collaborative Computational Project Number 4. The CCP4 suite: programs for protein crystallography. *Acta Crystallogr.* **1994**, *D50*, 760−763.

(33) Potterton, E.; Briggs, P.; Turkenburg, M.; Dodson, E. A graphical user interface to the CCP4 program suite. *Acta Crystallogr., Sect. D: Biol. Crystallogr.* **2003**, *59*, 1131−1137.

(34) Lu, J. P.; Chai, S. C.; Ye, Q. Z. Catalysis and inhibition of *Mycobacterium tuberculosis* methionine aminopeptidase. *J. Med. Chem.* **2010**, *53*, 1329−1337.

(35) Murshudov, G. N.; Vagin, A. A.; Dodson, E. J. Refinement of macromolecular structures by the maximum-likelihood method. *Acta Crystallogr., Sect. D: Biol. Crystallogr.* **1997**, *53*, 240−255.

(36) Emsley, P.; Cowtan, K. Coot: model-building tools for molecular graphics. *Acta Crystallogr., Sect. D: Biol. Crystallogr.* **2004**, *60*, 2126−2132.

(37) DeLano, W. L. *The PyMOL Molecular Graphics System*; Schrodinger, LLC: New York, 2002; http://www.pymol.org.